Revealing latent structural instabilities in perovskite ferroelectrics by layering and epitaxial strain: A first-principles study of Ruddlesden-Popper superlattices

S. M. Nakhmanson
Materials Science Division, Argonne National Laboratory, Argonne, Illinois 60439, USA
(Received 1 May 2008; revised manuscript received 16 July 2008; published 11 August 2008)

Utilizing first-principles computational techniques, we have mapped out structural instabilities in the Ruddlesden-Popper homologous oxide superlattice families with a general chemical formula $A_{n-1}A'_2\mathrm{Ti}_n\mathrm{O}_{3n+1}$, A=Sr, Ba, and Pb (perovskite-type slab) and A'=Sr (rocksalt-type insert) for n=1–5. Our calculations show that each superlattice family has a unique set of "instability footprints," combining the ferroelectric, antiferroelectric, and antiferrodistortive types, and that the competition among the instabilities can be influenced by epitaxial strain and changing thickness of the perovskite-type slab, granting us wide flexibility to fine tune the properties of these materials for various device applications.

DOI: 10.1103/PhysRevB.78.064107 PACS number(s): 77.84.Dy, 77.55.+f, 81.05.Zx

I. INTRODUCTION

The family of Ti-based perovskite oxides, which includes two prototypical ferroelectrics $BaTiO_3$ and $PbTiO_3$, is well known for its remarkable polar properties and has been thoroughly studied—both in its bulk and thin-film incarnations—during the past 60 years.[1] However, very recent advances in epitaxial engineering techniques, allowing one to create complex perovskite-oxide superlattices with numerous different-constituent layers and compositionally abrupt interfaces, have opened up a whole new dimension for a wide range of designer materials with highly tunable polar properties.[2] A synergistic approach to unravel the mysteries of such artificial structures, combining both experimental[3] and theoretical[4–7] efforts, has lead to discoveries of new phenomena that are not originally present in individual superlattice-component materials. These phenomena, for example, include an asymmetry of "up" and "down" polarizations due to the lack of inversion centers in some systems,[4,7] composition-induced polarization enhancement,[5–7] as well as an emergence of improper ferroelectricity.[8]

Still, stacking ABO_3 perovskite cells into superlattices is by far not the only recipe to obtain new functionality from the same constituent materials. For example, whole families of structures, or the so-called homologous series, can be created by layering perovskitelike slabs—and possibly alternating them with various structural blocks of other types—along certain crystallographic directions.[9,10] One of the most structurally simple series of such kind, an $A_{n+1}B_n\mathrm{O}_{3n+1}$ Ruddlesden-Popper (RP) homologous series,[11] is constructed by stacking $(n+\frac{1}{2})$-unit-cell-thick perovskite slabs in the [001] direction, with each new slab related to the previous one by a $(\frac{1}{2}a,\frac{1}{2}a)$ shift in the basal plane of the layered structure. An n=4 (n_4) member of the series is shown in Fig. 1(a) in its most symmetric (space group $I4/mmm$) phase containing two structural units per tetragonal unit cell. Although for large n the properties of the series converge to those of the "parent" ABO_3 structure—which is usually considered as an n_∞ member of the series—behavior of the low-n compounds can vary widely with increasing n, opening up yet another useful dimension for property control and customization. An extensively researched RP series for $SrRuO_3$ serves as a good example here, with n_1 member being an unconventional superconductor,[12] n_2 member exhibiting metamagnetism and quantum criticality,[13] and higher-n members being ferromagnets with rather complicated magnetic and transport properties.[14,15] Equally interesting examples could be drawn from RP series for $CaRuO_3$ (Ref. 16) or perovskite manganites.[17] As for perovskite titanates, where one would expect homologous series to possess interesting polar properties, only $CaTiO_3$ (Ref. 18) and $SrTiO_3$ have stable RP series, and only for the latter has a substantial number of the series members (n=1–5) been grown as high-quality epitaxial films.[19] Not surprisingly, none of these compounds exhibit pyroelectricity, ferroelectricity, or antiferroelectricity, and a hypothetical epitaxially stabilized ferro-

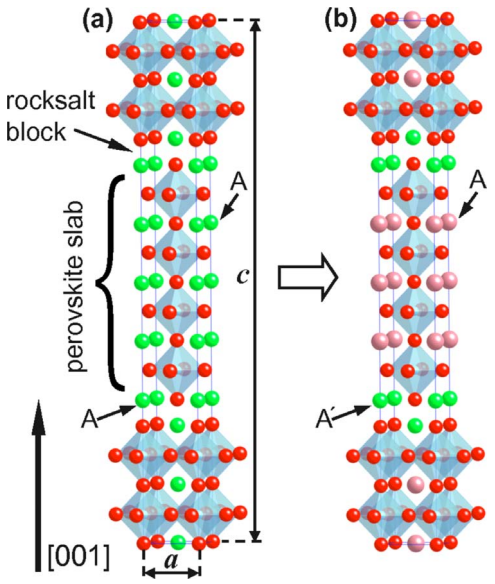

FIG. 1. (Color online) Crystal structure of a RP compound: (a) a conventional $A_{n+1}B_n\mathrm{O}_{3n+1}$ system (n=4); the lattice constants for the tetragonal cell are also shown. (b) an $A_{n-1}A'_2B_n\mathrm{O}_{3n+1}$ RP superlattice obtained from the previous structure by assigning different A-site ions to the perovskite and rocksalt units. BO_6 cages are represented by translucent octahedra, two varieties of A-site ions are shown in green (dark gray) and pink (light gray).

electric phase[20] of Pb_2TiO_4 has not yet been synthesized.

However, if we revisit the sample RP system in Fig. 1(a), we can envision an alternative route to obtain layered Ti-based materials with tunable electroactive properties. Since the geometry of this compound can be interpreted as a stacking of two kinds of structural units: the perovskite-type slabs and intermediate rocksalt-type blocks,[21] an expanded RP-series formula,[22] $A_{n-1}A'_2Ti_nO_{3n+1}$, can be written that supports different A-site ions in different units. Such ionic substitution does not break the $I4/mmm$ symmetry of the generic RP structure but rather morphs it into a superlattice-like object, shown in Fig. 1(b). We then fix the composition of the rocksalt-type insert (here we set $A'=$Sr), build up the perovskite-type slabs from stacks of ferroelectric $BaTiO_3$ or $PbTiO_3$ cells, and examine the behavior of the resulting RP superlattices in anticipation of interesting polar properties. The details of numerical techniques employed to analyze these structures are given below in Sec. II. We discuss the results of our calculations in Sec. III and make a few concluding remarks in Sec. IV.

II. COMPUTATIONAL DETAILS

In the current investigation we have studied three families of RP superlattices with $A=$Sr (regular RP series for $SrTiO_3$), Ba, and Pb. Since such compounds are currently being synthesized in the form of epitaxial thin films,[15,19] their strain state has a strong influence over their properties. Here we limited ourselves to only one potential substrate—cubic (c-) $SrTiO_3$, which is a popular choice for the growth of various perovskite materials. As it would be computationally prohibitive to do a detailed analysis of the polar properties for a large number of structures, we opted for a "wide brush-stroke" approach allowing us to quickly identify prospective candidate materials worthy of more thorough studies. Specifically, we mapped out structural instabilities for the high-symmetry $I4/mmm$ phases of $n=1-5$ members of each family at a small set of k points associated with polar, i.e., ferroelectric (FE) and antiferroelectric (AFE), and rotational, or antiferrodistortive (AFD), instabilities in perovskites.[23] A typical tetragonal unit cell for an RP compound, used for all the calculations presented here, is outlined in Fig. 1(a). It contains two structural $A_{n-1}Sr_2Ti_nO_{3n+1}$ units and is characterized by the in-plane lattice constant a and out-of-plane lattice constant c. A plane-wave density-functional-theory based method[24] with ultrasoft pseudopotentials[25] was utilized for the relaxation of ionic positions in the cell (with $4/mmm$ symmetry enforced), after which the phonon frequencies were computed at a particular k point with the help of a density-functional perturbation-theory (DFPT) approach.[26] Γ point,[27] as well as $X(\frac{1}{2},0,0)$, $M(\frac{1}{2},\frac{1}{2},0)$, $R(\frac{1}{2},0,\frac{1}{2})$, $Z(0,0,\frac{1}{2})$, and $A(\frac{1}{2},\frac{1}{2},\frac{1}{2})$, zone-boundary k points in the tetragonal Brillouin-zone (BZ) were sampled. Local-density approximation was used to account for exchange and correlations. The electronic wave-function and density plane-wave cutoffs were 30 and 300 Ry, respectively. $6\times6\times6$ and $6\times6\times1$ Monkhorst-Pack meshes[28] were employed for the BZ integrations in $ATiO_3$ and $A_{n-1}Sr_2Ti_nO_{3n+1}$ ($n>1$) systems, respectively. All the systems were considered to be at equilibrium when the Hellman-Feynman forces on the ions were less than 0.8×10^{-3} Ry/bohr ($\sim$0.02 eV/Å) and the $\sigma_{\alpha\alpha}$ components of the stress tensor were smaller than 0.5 kbar. To simulate the influence of strain in epitaxially grown structures, a was constrained to the theoretical lattice constant of c-$SrTiO_3$ ($a_s=3.851$ Å in this investigation) while c was allowed to vary.

III. RESULTS AND DISCUSSION

Before discussing the structural-instability competition and its implications in RP-titanate superlattices, it is instructive to briefly summarize what is known about the parent $ATiO_3$ structures. This information is assembled in Table I for $Pm\bar{3}m$ cubic (c-) $SrTiO_3$, $BaTiO_3$, and $PbTiO_3$, and in Table II for $P4/mmm$ (i.e., centrosymmetric and nonpolar) tetragonal $BaTiO_3$ and $PbTiO_3$, both relaxed to zero applied stress (t-) and epitaxially strained (et-) on c-$SrTiO_3$ substrate. Lattice constants for the cubic systems are included in Table I, while lattice constants and tetragonalities for the tetragonal systems are given in Table III (see entries for n_∞). Instability "characters," be those FE, AFE, or AFD, are listed in the tables together with their symmetry labels and associated imaginary frequencies, the latter indicating the instability strengths. Additionally, for tetragonal systems (Table II), where the [001] direction is symmetrically unequivalent to the [100] and [010], a subscript is used to provide a sense of direction. For the FE instabilities, where cations in each unit cell move against the oxygens, and for the AFE ones, where such cation displacements alternate between neighboring cells, this could be an axis (α) or a plane ($\alpha\beta$) of ionic motion. For the AFD instabilities, characterized by tilted octahedral oxygen cages, this could be a single (α) or an equivalent set (α,β) of rotational axes. As can be seen from Tables I and II, the Γ-point FE instability is dominating for both cubic and tetragonal phases of $BaTiO_3$, and $PbTiO_3$. In the $P4/mmm$ phase, the unstrained systems remain almost cubic, which leads to near degeneracies of FE_z and FE_{xy} modes at Γ, and AFE/AFD modes at other k points. All these degeneracies are lifted when epitaxial strain is applied, leading to additional softening of FE_z and hardening of FE_{xy} modes. However, in all the aforementioned cases, including the application of epitaxial strain, in addition to dominating FE instabilities we find other soft modes at the BZ boundaries [this result is in agreement with Ref. 23(b)], which are AFE in $BaTiO_3$ and AFD in $PbTiO_3$. All these instabilities disappear when the inversion symmetry in the $P4/mmm$ systems is broken and the FE soft modes are frozen in.

Structural parameters for the relaxed and epitaxially strained $Sr_{n+1}Ti_nO_{3n+1}$, $Ba_{n-1}Sr_2Ti_nO_{3n+1}$, and $Pb_{n-1}Sr_2Ti_nO_{3n+1}$ RP families are presented in Table III, with data for c-$SrTiO_3$ and $P4/mmm$ $BaTiO_3$, and $PbTiO_3$ included in place of the n_∞ members of the appropriate series. As shown in the last column of the table, epitaxial growth on the c-$SrTiO_3$ substrate causes biaxial compression in Ba- and Pb-based RP superlattices and slight biaxial tension, which

TABLE I. Lattice constants and soft phonon frequencies ω (cm^{-1}) at k points Γ, X, M, and R for $Pm\bar{3}m$ (c-) $SrTiO_3$, $BaTiO_3$, and $PbTiO_3$ relaxed to zero applied stress.

		$\Gamma(0,0,0)$		$X(\frac{1}{2},0,0)$		$M(\frac{1}{2},\frac{1}{2},0)$		$R(\frac{1}{2},\frac{1}{2},\frac{1}{2})$	
System	a (Å)	Label	ω	Label	ω	Label	ω	Label	ω
$SrTiO_3$	3.851					B_{1g} (AFD)	$28i$	T_{2u} (AFD)	$90i$
$BaTiO_3$	3.936	T_{1u} (FE)	$148i$	E_g (AFE)	$90i$	B_{1u} (AFE)	$55i$		
$PbTiO_3$	3.878	T_{1u} (FE)	$131i$			B_{1g} (AFD)	$52i$	T_{2u} (AFD)	$83i$

tends to disappear completely with increasing n, in Sr-based structures.[29]

Turning to the instability analysis, the phonon calculations show that members of all the three families exhibit structural instabilities when confined to high-symmetry $I4/mmm$ phase. Furthermore, each series has a unique set of soft modes, including the FE, AFE, and AFD types. The evolution of the leading instability strengths at various k points in the three families with increasing n is shown in panels (a), (b), and (c) of Fig. 2, respectively. Results for both relaxed and epitaxially strained on c-$SrTiO_3$ systems are presented.

With the exception of the n_2 series member, which has no structural instabilities, the structures belonging to the Sr-based family possess only rotational instabilities with AFD_z-type soft modes at M and A being the most prominent. Both of these instabilities are represented by the same curve in Fig. 2(a) because for the family members with $n>2$ their frequencies are always nearly degenerate [the same is done for degenerate $\omega(n)$ dependencies in the Ba- and Pb-based families in panels (b) and (c)]. The ionic-displacement motifs for both modes consist of oxygen-octahedron cage rotations around the [001] direction with consecutive layers of cages moving in antiphase. Not surprisingly, for large n these displacement patterns converge to the R-point T_{2u} AFD soft mode in c-$SrTiO_3$. For the epitaxially strained structures, only very small mode-frequency shifts were found due to almost perfect in-plane lattice constant match between the series members and the substrate.

The structures from the Ba-based family [Fig. 2(b)], again with the exception of the n_2 member that is stable both with and without the applied strain, display a much more unusual behavior. In their unstrained states they are either stable (n_3 member) or have a mixture of FE and AFE instabilities that are all polarized in the xy plane. In the $FE_{xy}(\Gamma)$ mode, A- and B-site cations in both perovskite slabs in the cell move in unison against their oxygen cages. In the $AFE_{xy}(\Gamma)$ mode, the directions of such FE slab displacements are antiparallel for the first and the second slabs, while in the $AFE_{xy}(Z)$ mode, the FE displacements have the same direction in two consecutive slabs with the two neighboring slabs moving in the opposite direction. The frequencies of all these nodes are fairly close for the n_4 system and become nearly degenerate in the n_5 system. However, when epitaxial strain is applied, the xy-plane instabilities in every system disappear in favor of AFE_z ones. In these modes, unit-cell-width columns with the same [001]-polarized displacement motifs alternate along [100] for X and R or along [110] for M and A, with the mode frequencies being degenerate for each pair of k points.

Finally, the Pb-based family [Fig. 2(c)] possesses the richest set of structural instabilities, consisting of the FE_{xy} and AFE_{xy} ones, like those of the Ba-based compounds, and AFD_z ones, like those of the Sr-based compounds. Only the n_2 member of the series, which has one layer of PbO per perovskite slab, is entirely free of rotational instabilities; however, the following member does exhibit the FE, AFE, and AFD types, with the latter one being the strongest. For the unstrained n_4 compound, though, all the three instabilities have nearly equal strengths and for $n=5$ the situation becomes the opposite of the n_3 system. Since the influence of epitaxial strain is not as pronounced in this family, as it is in the Ba-based structures, the FE_{xy} and AFE_{xy} instabilities do not disappear completely when the series members are lattice matched to the substrate. Still, these modes are hardened by

TABLE II. Soft-phonon frequencies ω (cm^{-1}) for the relaxed to zero stress (t-) and epitaxially strained on c-$SrTiO_3$ (et-) $P4/mmm$ $BaTiO_3$ and $PbTiO_3$ at k points Γ, X, M, R, Z, and A. Epitaxial strain $\epsilon=a_s/a-1=-2.16$ and -0.7% for et-$BaTiO_3$ and et-$PbTiO_3$, respectively.

	$\Gamma(0,0,0)$		$X(\frac{1}{2},0,0)$		$M(\frac{1}{2},\frac{1}{2},0)$		$R(\frac{1}{2},0,\frac{1}{2})$		$Z(0,0,\frac{1}{2})$		$A(\frac{1}{2},\frac{1}{2},\frac{1}{2})$	
System	Label	ω	Label	ω	Label	ω	Label	ω	Label	ω	Label	ω
t-$BaTiO_3$	A_{2u} (FE_z)	$149i$	B_{2g} (AFE_z)	$91i$	B_{1u} (AFE_z)	$55i$	A_2 (AFE_{xy})	$55i$	E (AFE_{xy})	$91i$		
	E_u (FE_{xy})	$148i$	B_{1g} (AFE_{xy})	$91i$								
et-$BaTiO_3$	A_{2u} (FE_z)	$219i$	B_{2g} (AFE_z)	$175i$	B_{1u} (AFE_z)	$142i$						
t-$PbTiO_3$	A_{2u} (FE_z)	$131i$			B_{1g} (AFD_z)	$52i$	A_1 ($AFD_{x,y}$)	$52i$			E ($AFD_{x,y}$)	$83i$
	E_u (FE_{xy})	$131i$									B_1 (AFD_z)	$83i$
et-$PbTiO_3$	A_{2u} (FE_z)	$148i$			B_{1g} (AFD_z)	$77i$	A_1 ($AFD_{x,y}$)	$40i$			B_1 (AFD_z)	$99i$
	E_u (FE_{xy})	$112i$									E ($AFD_{x,y}$)	$79i$

TABLE III. Structural parameters for the relaxed to zero stress and epitaxially strained on c-$SrTiO_3$ $I4/mmm$ $A_{n-1}Sr_2Ti_nO_{3n+1}$ RP superlattices. a_s=3.851 Å. Epitaxial strain $\epsilon=a_s/a-1$.

System	n	a (Å)	c/a	c_ϵ/a_s	ϵ (%)
$Sr_3Ti_2O_7$	2	3.843	5.207	5.191	0.21
$Sr_4Ti_3O_{10}$	3	3.847	7.199	7.187	0.10
$Sr_5Ti_4O_{13}$	4	3.848	9.196	9.189	0.08
$Sr_6Ti_5O_{16}$	5	3.849	11.196	11.186	0.05
c-$SrTiO_3$	∞	3.851	1.000	1.000	0.00
$BaSr_2Ti_2O_7$	2	3.886	5.195	5.275	−0.90
$Ba_2Sr_2Ti_3O_{10}$	3	3.903	7.186	7.352	−1.33
$Ba_3Sr_2Ti_4O_{13}$	4	3.912	9.179	9.429	−1.56
$Ba_4Sr_2Ti_5O_{16}$	5	3.917	11.177	11.506	−1.68
t-$BaTiO_3$	∞	3.936	1.0001	1.038	−2.16
$PbSr_2Ti_2O_7$	2	3.856	5.209	5.221	−0.13
$Pb_2Sr_2Ti_3O_{10}$	3	3.864	7.203	7.246	−0.34
$Pb_3Sr_2Ti_4O_{13}$	4	3.868	9.200	9.272	−0.44
$Pb_4Sr_2Ti_5O_{16}$	5	3.870	11.198	11.297	−0.49
t-$PbTiO_3$	∞	3.878	1.0001	1.013	−0.70

the application of strain; on the other hand, the AFD_z modes are softened even more. This removes the degeneracy for the n_4 system, making the AFD_z instability more preferable, and *inverts* the mode dominance in the n_5 system, switching it from the FE_{xy}/AFE_{xy} to the AFD_z-preferred state.

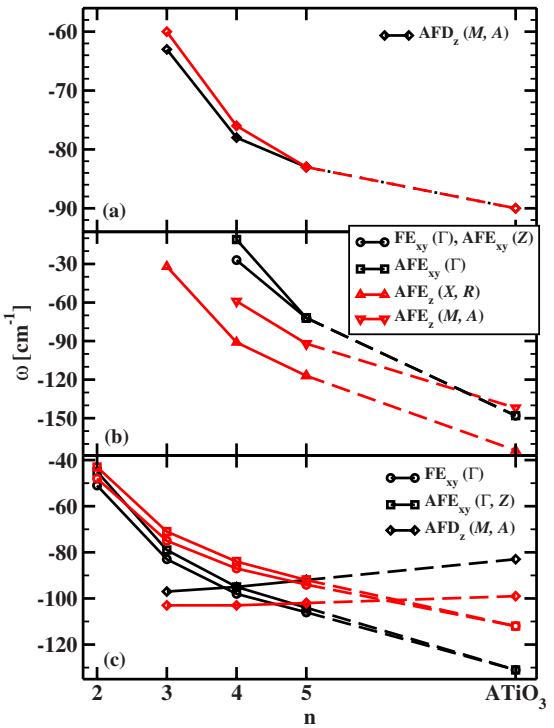

FIG. 2. (Color online) Evolution of the soft-mode frequencies at various k points in the RP-superlattice families with increasing thickness of perovskite slab n: (a) $Sr_{n+1}Ti_nO_{3n+1}$, (b) $Ba_{n-1}Sr_2Ti_nO_{3n+1}$, and (c) $Pb_{n-1}Sr_2Ti_nO_{3n+1}$. The strain state of a superlattice is represented by the color (shade) of a curve: black refers to relaxed systems and red (dark gray) to systems epitaxially strained on c-$SrTiO_3$ substrate. $\omega(n)$ dependencies at different k points that have degenerate or nearly degenerate frequencies are shown by the same curves.

IV. CONCLUSIONS

Summarizing our observations, we can claim that the presence of the rocksalt-type inserts in the RP superlattices *does not* support polar instabilities polarized along [001]. Furthermore, the application of compressive epitaxial strain discourages ferroelectricity in the xy plane as well. With their FE instabilities utterly destroyed, the strained systems have to utilize *the next latent instability available in the parent structure* to lower their energy. That makes Ba-based compounds predisposed to antiferroelectricity (and thus an attractive choice for energy-storage applications) and Pb-based ones to antiferrodistortiveness with the n_2 system still likely to be an in-plane ferroelectric. Naturally, since in the present investigation we analyze only soft-mode competition trends in these structures, a much more thorough (and computationally costly) work is required to determine their true ground states.

In closing, we comment on the feasibility of synthesizing these structures. So far, there has been one report of a similar Mn-based layered superlattice being made using molecular-beam epitaxy (MBE).[30] The quoted above work on MBE growth of RP series for $SrRuO_3$ (Ref. 15) and $SrTiO_3$ (Ref. 19) is equally encouraging. We hope that our predictions will stimulate further experimental effort to grow such layered Ti-based perovskite-oxide superlattices and study their polar properties.

ACKNOWLEDGMENTS

This project was supported under Contract No. DE-AC02-06CH11357 between UChicago Argonne, LLC, and the Department of Energy. The author is grateful to Dillon Fong, Peter Zapol, Seungbum Hong, Amanda Petford-Long, and Orlando Auciello for many fruitful discussions.

[1] M. E. Lines and A. M. Glass, *Principles and Applications of Ferroelectrics and Related Materials* (Oxford University Press, New York, 1977).

[2] D. G. Schlom, L.-Q. Chen, C.-B. Eom, K. M. Rabe, S. K. Streiffer, and J.-M. Triscone, Annu. Rev. Mater. Res. **37**, 589 (2007).

[3] H. Yamada, M. Kawasaki, Y. Ogawa, and Y. Tokura, Appl. Phys. Lett. **81**, 4793 (2002); M. P. Warusawithana, E. V. Colla, J. N. Eckstein, and M. B. Weissman, Phys. Rev. Lett. **90**, 036802 (2003); H. N. Lee, H. M. Christen, M. F. Chisholm, C. M. Rouleau, and D. H. Lowndes, Nature (London) **433**, 395 (2005); M. Dawber, C. Lichtensteiger, M. Cantoni, M. Veithen, P. Ghosez, K. Johnston, K. M. Rabe, and J.-M. Triscone, Phys. Rev. Lett. **95**, 177601 (2005); D. A. Tenne, A. Bruchhausen, N. D. Lanzillotti Kimura, A. Fainstein, R. S. Katiyar, A. Cantarero, A. Soukiassian, V. Vaithyanathan, J. H. Haeni, W. Tian, D. G. Schlom, K. J. Choi, D. M. Kim, C.-B. Eom, H. P. Sun, X. Q. Pan, Y. L. Li, L. Q. Chen, Q. X. Jia, S. M. Nakhmanson, K. M. Rabe, and X. X. Xi, Science **313**, 1614 (2006).

[4] N. Sai, B. Meyer, and D. Vanderbilt, Phys. Rev. Lett. **84**, 5636 (2000).

[5] J. B. Neaton and K. M. Rabe, Appl. Phys. Lett. **82**, 1586 (2003).

[6] K. Johnston, X. Huang, J. B. Neaton, and K. M. Rabe, Phys. Rev. B **71**, 100103(R) (2005).

[7] S. M. Nakhmanson, K. M. Rabe, and D. Vanderbilt, Appl. Phys. Lett. **87**, 102906 (2005); Phys. Rev. B **73**, 060101(R) (2006).

[8] E. Bousquet, M. Dawber, N. Stucki, C. Lichtensteiger, P. Hermet, S. Gariglio, J.-M. Triscone, and P. Ghosez, Nature (London) **452**, 732 (2008).

[9] Y. Tokura and T. Arima, Jpn. J. Appl. Phys., Part 1 **29**, 2388 (1990).

[10] K. S. Aleksandrov and V. V. Beznosikov, Fiz. Tverd. Tela (S.-Peterburg) **39**, 785 (1997) [Phys. Solid State **39**, 695 (1997)].

[11] S. N. Ruddlesden and P. Popper, Acta Crystallogr. **10**, 538 (1957); **11**, 54 (1958).

[12] Y. Maeno, H. Hashimoto, K. Yoshida, S. Nishizaki, T. Fujita, J. G. Bednorz, and F. Lichtenberg, Nature (London) **372**, 532 (1994); K. Ishida, H. Mukuda, Y. Kitaoka, K. Asayama, Z. Q. Mao, Y. Mori, and Y. Maeno, *ibid.* **396**, 658 (1998); A. P. Mackenzie and Y. Maeno, Rev. Mod. Phys. **75**, 657 (2003).

[13] R. S. Perry, L. M. Galvin, S. A. Grigera, L. Capogna, A. J. Schofield, A. P. Mackenzie, M. Chiao, S. R. Julian, S. I. Ikeda, S. Nakatsuji, Y. Maeno, and C. Pfleiderer, Phys. Rev. Lett. **86**, 2661 (2001); S. A. Grigera, R. S. Perry, A. J. Schofield, M. Chiao, S. R. Julian, G. G. Lonzarich, S. I. Ikeda, Y. Maeno, A. J. Millis, and A. P. Mackenzie, Science **294**, 329 (2001); S. A. Grigera, P. Gegenwart, R. A. Borzi, F. Weickert, A. J. Schofield, R. S. Perry, T. Tayama, T. Sakakibara, Y. Maeno, A. G. Green, and A. P. Mackenzie, *ibid.* **306**, 1154 (2004).

[14] G. Cao, S. K. McCall, J. E. Crow, and R. P. Guertin, Phys. Rev. B **56**, R5740 (1997); G. Cao, L. Balicas, W. H. Song, Y. P. Sun, Y. Xin, V. A. Bondarenko, J. W. Brill, S. Parkin, and X. N. Lin, *ibid.* **68**, 174409 (2003); D. Fobes, M. H. Yu, M. Zhou, J. Hooper, C. J. O'Connor, M. Rosario, and Z. Q. Mao, *ibid.* **75**, 094429 (2007).

[15] W. Tian, J. H. Haeni, D. G. Schlom, E. Hutchinson, B. L. Sheu, M. M. Rosario, P. Schiffer, Y. Liu, M. A. Zurbuchen, and X. Q. Pan, Appl. Phys. Lett. **90**, 022507 (2007).

[16] G. Cao, S. McCall, M. Shepard, J. E. Crow, and R. P. Guertin, Phys. Rev. B **56**, R2916 (1997); M. Braden, G. André, S. Nakatsuji, and Y. Maeno, *ibid.* **58**, 847 (1998); A. V. Puchkov, M. C. Schabel, D. N. Basov, T. Startseva, G. Cao, T. Timusk, and Z.-X. Shen, Phys. Rev. Lett. **81**, 2747 (1998); I. I. Mazin and D. J. Singh, *ibid.* **82**, 4324 (1999); D. J. Singh and S. Auluck, *ibid.* **96**, 097203 (2006); W. Bao, Z. Q. Mao, Z. Qu, and J. W. Lynn, *ibid.* **100**, 247203 (2008).

[17] See, e.g., J. F. Mitchell, D. N. Argyriou, A. Berger, K. E. Gray, R. Osborn, and U. Welp, J. Phys. Chem. B **105**, 10731 (2001).

[18] M. M. Elcombe, E. H. Kisi, K. D. Hawkins, T. J. White, P. Goodman, and S. Matheson, Acta Crystallogr., Sect. B: Struct. Sci. **47**, 305 (1991).

[19] J. H. Haeni, C. D. Theis, D. G. Schlom, W. Tian, X. Q. Pan, H. Chang, I. Takeuchi, and X.-D. Xiang, Appl. Phys. Lett. **78**, 3292 (2001); W. Tian, X. Q. Pan, J. H. Haeni, and D. G. Schlom, J. Mater. Res. **16**, 2013 (2001).

[20] C. J. Fennie and K. M. Rabe, Phys. Rev. B **71**, 100102(R) (2005).

[21] $R_1(+\beta)$ in the notation of Ref. 10.

[22] B. V. Beznosikov and K. S. Aleksandrov, Kristallografiya **45**, 864 (2000) [Crystallogr. Rep. **45**, 792 (2000)].

[23] The instability analysis has been widely used by various authors to identify likely low-energy phases of perovskite materials, as well as to gain other useful insights into their behavior. See, e.g., (a) D. J. Singh, Phys. Rev. B **52**, 12559 (1995); (b) P. Ghosez, E. Cockayne, U. V. Waghmare, and K. M. Rabe, *ibid.* **60**, 836 (1999); (c) M. Fornari and D. J. Singh, *ibid.* **63**, 092101 (2001).

[24] We used PWSCF code (available from http://www.pwscf.org) for the calculations presented here.

[25] D. Vanderbilt, Phys. Rev. B **41**, 7892 (1990).

[26] S. Baroni, S. de Gironcoli, A. Dal Corso, and P. Giannozzi, Rev. Mod. Phys. **73**, 515 (2001).

[27] We disregard the depolarizing-field effects in our calculations assuming that this field is screened by top and bottom electrodes.

[28] H. J. Monkhorst and J. D. Pack, Phys. Rev. B **13**, 5188 (1976).

[29] These strains should be achievable experimentally for any n since they are capped from above by strains in *et*-$BaTiO_3$ and *et*-$PbTiO_3$, both of which are routinely grown on *c*-$SrTiO_3$.

[30] H. Tanaka and T. Kawai, Appl. Phys. Lett. **76**, 3618 (2000).